Photodissociation of Acrylic Acid at 193 nm

D. C. Kitchen, N. R. Forde, and L. J. Butler*

The James Franck Institute and Department of Chemistry, The University of Chicago, Chicago, Illinois 60637

Received: December 16, 1996; In Final Form: March 24, 1997[⊗]

This paper describes the photolysis of acrylic acid (H_2C═CHCOOH) monomers upon $\pi \rightarrow \pi^*$ excitation at 193 nm. The photofragment velocity distribution measurements indicate that only primary C−C and C−O bond fissions are major photodissociation pathways; molecular decarboxylation and decarbonylation reactions do not occur to a significant extent. There are two different primary C−C bond fission channels resulting in the production of HOCO radicals in the ground and first electronically excited states. We also determine an upper limit on the C−C bond strength of about 100 kcal/mol; this agrees with the value we calculate from literature heats of formation but is considerably less than that assumed by previous workers.

Introduction

The combustion reaction OH + CO → H + CO_2 is of great interest because of its role in the oxidation of fossil fuels and in atmospheric reactions. The intermediate complex in this reaction is *trans*-HOCO, so examination of the chemical reactions and photophysics of this radical are important in order to gain a better understanding of combustion and atmospheric processes. Several studies on the HOCO radical have used the photodissociation of small carboxylic acids (most notably acetic[1] and acrylic acid[2,3]) in order to generate the HOCO species.

While several workers have studied the photodissociation dynamics of acetic acid, little is known about acrylic acid, H_2C═CHCOOH, photolysis, especially about the quantum yield of HOCO (or other products) and the energy disposal to relative kinetic energy versus internal energy of the photofragments. Although most work on acrylic acid has focused on polymerization reactions, several processes have been proposed as primary dissociation pathways:

$$H_2C{=}CHCOOH + h\nu \rightarrow H_2C{=}CH + HOCO \quad (1)$$

$$\rightarrow H_2C{=}CHCO + OH \quad (2)$$

$$\rightarrow H_2C{=}CH_2 + CO_2 \quad (3)$$

$$\rightarrow H_2C{=}COH + CO \quad (4)$$

Reactions 1 and 2 yield radical products from simple C−C and C−O bond cleavage respectively; eq 3 represents decarboxylation, and eq 4 is a decarbonylation reaction.

Early pyrolysis studies[4] suggested that reactions 3 and 4 were the primary dissociation route of simple olefinic acids. Although simple thermally induced decomposition does not necessarily result in the same products as does excited state dissociation, these reactions are noteworthy because analogous reactions have been observed for α,β-unsaturated aldehydes,[5−7] compounds which are similar to acrylic acid. There have been few gas-phase experiments on acrylic acid using monochromatic light. Singleton *et al.*[8] determined the OH quantum yield upon 222 nm irradiation (exciting the $n \rightarrow \pi^*$ transition) to be 0.148 ± 0.090 at room temperature and 0.341 ± 0.014 at 100 °C. These values are much smaller than those they obtained for formic and acetic acids, indicating the importance of other photodissociation pathways in acrylic acid. On the basis of the observation of intense infrared fluorescence in the spectral region corresponding to the CO_2 asymmetric stretch after 193 nm excitation of acrylic acid, Rosenfeld and Weiner claim that decarboxylation is a primary dissociation pathway.[9] Finally, Miyoshi and co-workers[3] suggest on the basis of mass spectral evidence that, in addition to C−C bond fission, reactions 2 and 4 occur after excitation at 193 nm.

The above studies yield conflicting results, and there is little information on the important C−C fission pathway that produces the HOCO radical. In order to better characterize the photodynamics of acrylic acid, this work explores the dissociation of this molecule photoexcited via the $\pi\pi^*$ transition at 193 nm. We measure the photofragment velocities with a crossed laser−molecular beam apparatus in order to determine the primary photodissociation pathways and energy imparted to translational kinetic energy of the resultant fragments for each pathway. Comparisons to other similar systems are also made in order to better explain the observed dynamics.

Experimental Method

We measure the fragment velocities from the photodissociation of acrylic acid with a crossed laser−molecular beam apparatus.[10] After photodissociation with a pulsed excimer laser, neutral dissociation products scatter from the crossing point of the laser and the molecular beam with velocities determined by the vector sum of the molecular beam velocity and the recoil velocity imparted during dissociation. Fragments scattered into the 1.5° acceptance angle of the detector travel 44.13 cm and are ionized by 200 eV electrons. After mass selection with a quadrupole mass filter, the ions are counted with a Daly detector and multichannel scaler with respect to their time-of-flight (TOF) from the interaction region after the dissociating laser pulse. Upon subtraction of the calibrated ion flight time ($4.69 m_{ion}^{1/2}$ in units of μs), forward convolution fitting of the TOF spectrum determines the distribution of energies released to relative product translation in the dissociation.

The molecular beam was formed by expanding the gaseous sample seeded in He to give a total stagnation pressure of either 300 or 340 Torr depending upon nozzle size used. Acrylic acid inhibited with 200 ppm hydroquinone monomethyl ether was used as received from Aldrich. Heated in a constant temperature bath set to 40 °C, the sample gives a partial pressure of 10.5 Torr.[11] Due to equipment problems, two different nozzles were used during the course of this work. We performed low nozzle temperature experiments by heating a 0.094 mm diameter nozzle

[⊗] Abstract published in *Advance ACS Abstracts,* July 15, 1997.

S1089-5639(97)00024-8 CCC: $14.00

to 120 °C; the nozzle temperature was measured with a chromel−alumel thermocouple placed in contact with the nozzle tip. A total stagnation pressure of 300 Torr was used for these studies, resulting in a 3.6% beam in helium. For most of the data presented herein, we used a 0.066 mm diameter nozzle heated to 375 °C to destroy clusters that are inherent to the acrylic acid vapor. In order to improve the supersonic expansion from the smaller nozzle diameter, we used a total stagnation pressure of 340 Torr for these studies, resulting in a 3.2% beam in helium. Note that heating the smaller diameter nozzle to 120 °C yielded results similar to those obtained with the larger nozzle. Typical mean beam velocities were 1.7×10^5 cm/s with a full-width-at-half-maximum (fwhm) of 21% for 375 °C nozzle temperature studies and 1.4×10^5 cm/s with a fwhm of 17% for the lower temperature work. To measure the velocity of the parent molecular beam *in situ*, the molecular beam source was rotated to point into the detector and a chopper wheel raised into the beam. To measure the velocities of the neutral photofragments, the molecular beam source is rotated to various angles in the plane containing the beam and detector axis, a plane perpendicular to the laser beam propagation direction. The molecular beam source angle is given here with respect to the detector axis.

A Lumonics PM848 excimer laser filled with ArF produced the 193 nm light used to photodissociate the acrylic acid molecules. The output pulse energy was power-locked to 20 mJ/pulse and attenuated with a fine-mesh wire screen. The light was focused to a 5 mm^2 spot size at the crossing region of the laser and molecular beam, and attenuated laser power averaged 5 mJ/pulse in this interaction region. Preliminary experiments at both higher and lower laser power showed no significant difference in the signal observed, so multiphoton effects are not present in data reported here. Quadrupole resolution was adjusted to between 0.9 and 1.0 amu fwhm for all masses.

In experiments on acrylic acid, the presence of clusters in the vapor can have a large effect on the photodissociation dynamics. In the condensed phase, acrylic acid, like all carboxylic acids, forms strong hydrogen bonds between monomer units, resulting in very stable clusters. It is this property which accounts for the higher boiling point for these compounds than would be predicted on the basis of molecular weight alone. Even in the gas phase, however, these hydrogen bonds remain intact and result in significant dimer and higher order cluster contributions to the vapor. In formic acid, HCOOH, clusters comprise upward of 95% of the vapor at room temperature and pressure.[12] Even though acrylic acid vapor is likely to contain a lower percentage of clusters, the unusually high binding energy due to the hydrogen bonds (15.2 kcal/mol in gaseous formic acid[13]) results in large cluster contributions to the molecular beam, even at nozzle temperatures of 120 °C. Only by increasing the nozzle temperature to about 375 °C were we able to greatly reduce, but not eliminate, clusters from the expansion. It is not practical to use temperatures much higher than this in our apparatus. We should note that lowering the partial pressure of acrylic acid in the initial beam expansion has little effect on the relative cluster/monomer ratio, therefore, the large cluster contribution must be inherent to the acrylic acid vapor and not from clusters formed in the supersonic expansion.

In order to determine the extent of cluster contamination, we integrated the parent molecular beam TOF at two different mass/charge ratios. Acrylic acid monomer yields the largest ion signal at its parent ion, $m/e^+ = 72$, while clusters give a large signal at $m/e^+ = 73$. Although we cannot give an absolute measure of the amount of clusters in the beam at a given temperature because daughter ion fragmentation patterns are unknown, we can determine the relative amount of cluster reduction achieved by heating the nozzle.

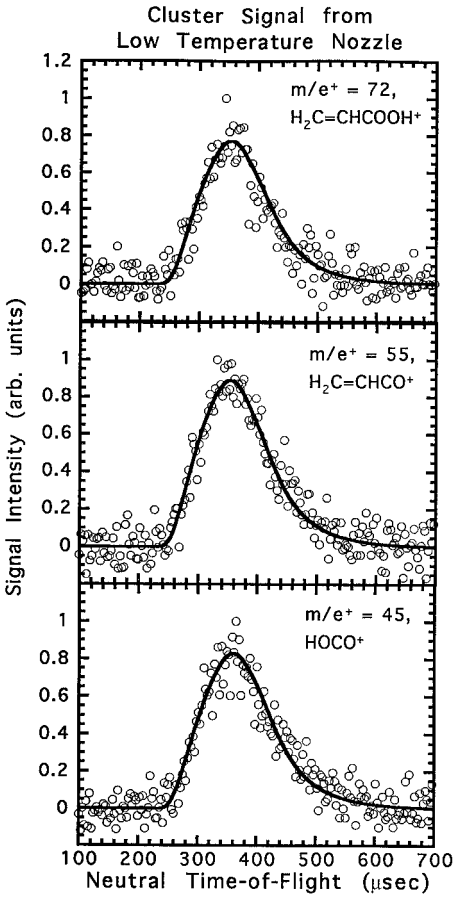

Figure 1. Laboratory time-of-flight spectra at the $m/e^+ = 72$, $H_2C{=}CHCOOH^+$ (top), $m/e^+ = 55$, $H_2C{=}CHCO^+$ (middle), and $m/e^+ = 45$, $HOCO^+$ (bottom) daughter ions of photofragments resulting from the 193 nm photodissociation of acrylic acid clusters. The nozzle was heated to 120 °C, and the source angle was 10°. The signal at all three mass/charge ratios has the same flight time from the laser−molecular beam interaction region to the ionizer and so must result from the same radical produced by the photodissociation event. Because the top frame represents the signal collected at the parent ion of acrylic acid and the molecular beam is rotated 10° from the detector axis, only cluster dissociation resulting in heavy photofragments can produce this signal. For this figure only, we subtracted the ion flight time of $4.69m_{ion}^{1/2}$ (in units of μs) from the total flight time recorded in the original data; then one can easily see that the neutral flight times of the signal at all three ion masses are identical.

Results and Analysis

A. Low Nozzle Temperature Data: Cluster Photodissociation. Figure 1 shows the photofragment time-of-flight (TOF) spectra collected at $m/e^+ = 72$, $H_2C{=}CHCOOH^+$ (top), $m/e^+ = 55$, $H_2C{=}CHCO^+$ (middle), and $m/e^+ = 45$, $HOCO^+$ (bottom), taken at a source angle of 10° and with a nozzle temperature of 120 °C. Note that we subtract ion flight time from this plot in order to show that the signal in each spectrum results from the same neutral fragment. We also observed a signal corresponding to the same arrival times at $m/e^+ = 44$, 27, 26 and 17, and there is probably a signal from cluster dissociation at other mass/charge ratios not investigated. These spectra all appear identical, and since $m/e^+ = 72$ is the parent mass of acrylic acid, all of the signal at this mass/charge ratio must be due to cluster dissociation. We fit the data in Figure 1 to determine the recoil velocity, relative to the center-of-mass velocity, of the heavier of the two photofragments from the dissociation of clusters. This relative recoil velocity distribution,

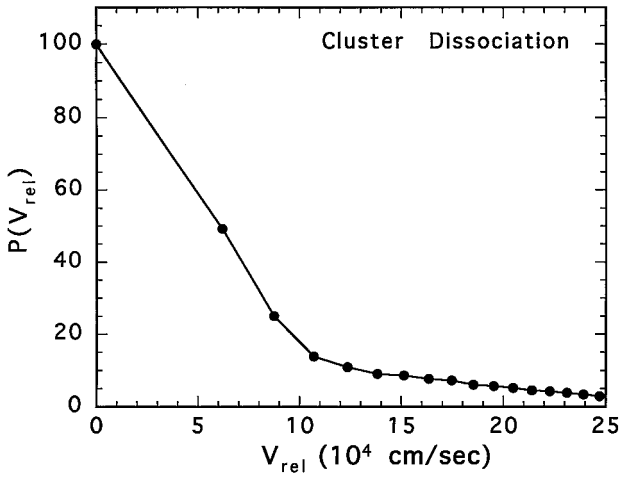

Figure 2. Relative recoil velocities (v_{rel}) of the heavy fragments resulting from acrylic acid cluster photodissociation. The distribution is derived from forward convolution fitting the signal in Figure 1 as discussed in the text. This distribution was used to fit the signal from cluster dissociation in all the other TOF spectra in this paper.

$P(v_{rel})$, is shown in Figure 2. We can use this distribution in order to identify what signal in the data in the next section (taken with a high-temperature nozzle) is due to clusters.

In the next section we heat the nozzle to a much higher temperature to reduce the amount of clusters in the molecular beam. Although in the low nozzle temperature data there is a signal due to monomer dissociation in several of the spectra, most notably in the CO_2^+ and OH^+ data, it is small compared to the signal resulting from cluster dissociation. Much of the signal from clusters also overlaps the signal from monomers. Thus, in order to accurately determine dissociation pathways in acrylic acid, we had to greatly increase the nozzle temperature. In order to illustrate that the dissociation pathways and translational energy distributions determined in the next section are also applicable to data taken with a low nozzle temperature, we will return to the 120 °C nozzle temperature data in section C below.

B. High Nozzle Temperature Data: Monomer Photodissociation. By increasing the nozzle temperature from 120 to 375 °C, we reduce the amount of clusters relative to monomer molecules in the beam by a factor of 3. We determine the amount of reduction by measuring the relative signal intensity of $m/e^+ = 72$ (monomers) to $m/e^+ = 73$ (clusters) in the molecular beam. We now present all the TOF data and assignments, referring the reader to section D for the reasons we assign a signal to a particular photofragment even though we do not observe a signal at the parent mass/charge ratio of said photofragment. Figure 3 shows the photofragment TOF spectrum collected at $m/e^+ = 44$, CO_2^+, after 600 000 laser shots with a source angle of 20°. At this large angle, the signal due to the photodissociation of clusters cannot contribute to the spectrum because of their small recoil angle from the interaction region. We assign the signal in Figure 3 to the CO_2^+ daughter ion of the primary C−C bond fission product HOCO (eq 1) because the same photofragments give a signal at OH^+. Through forward convolution fitting of the data we derive the overlapping center-of-mass (c.m.) translational energy distributions, $P(E_T)$'s, depicted in Figure 4. (Spectra at other mass/charge ratios are obviously bimodal, so we fit the CO_2^+ spectra to two C−C bond fission channels.) One distribution peaks at 6.0 kcal/mol with a high-energy tail that extends to about 28 kcal/mol; the other has $E_{mean} = 27.5$ kcal/mol. Standard heats of formation data[14] give a C−C bond dissociation energy of about 94 kcal/mol; the high-energy portion of our measured kinetic energy distribution extends to within a few kcal/mol of

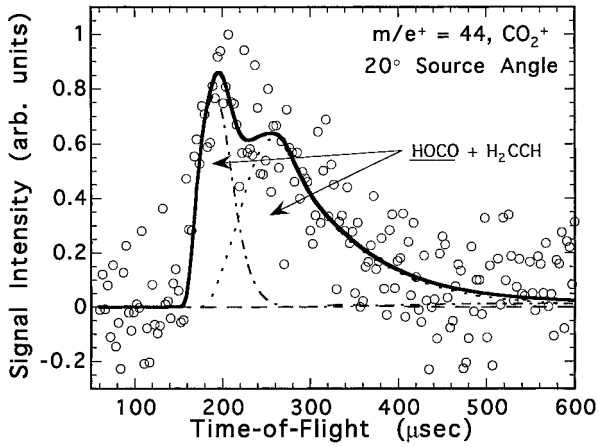

Figure 3. Laboratory time-of-flight spectrum of the photofragments detected at the $m/e^+ = 44$, CO_2^+, daughter ion of the HOCO photofragments. The source angle was 20°, and the nozzle was heated to 375 °C. All the signal results from primary C−C bond fission with two different translational energy distributions and is fit with the $P(E_T)$'s shown in Figure 4 with a high:low translational energy distribution ratio of 2.0:1.0.

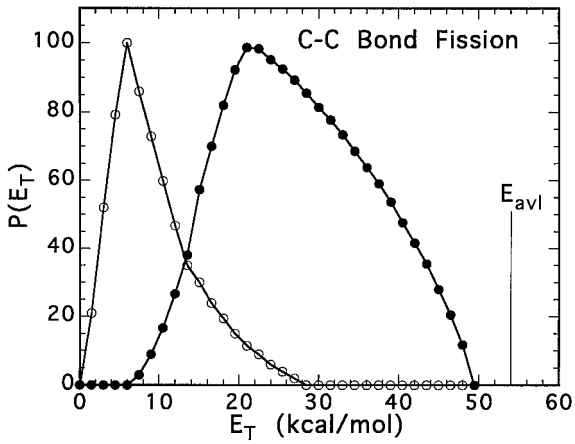

Figure 4. Center-of-mass product translational energy distributions, $P(E_T)$'s, for the C−C bond fission channels in acrylic acid. The $P(E_T)$'s are derived from forward convolution fitting the CO_2^+ signal in Figure 3. The need for two different $P(E_T)$'s is discussed in section E. The line at 54 kcal/mol represents the energy available after photodissociation based on a C−C bond strength of 94 kcal/mol calculated from heats of formation. Note that we observe some photofragments with nearly all of the available energy partitioned into relative translational motion of the photoproducts.

the 54 kcal/mol of available energy calculated with this bond energy. (The sharp cutoff of the $P(E_T)$ at 50 rather than 54 kcal/mol suggests the C−C bond energy calculated from literature heats of formation may be a few kcal/mol too small; this is understandable given the uncertainty in the published heats of formation for the radical species.) This is not simply a bimodal energy distribution, as the relative weightings of the two channels must be varied in order to fit the signal obtained at other mass/charge ratios. Thus, it is clear that the HOCO product for one channel has a different daughter ion production probability than the HOCO product for the second channel. We assign the slower moving fragments to a channel which produces electronically excited HOCO radicals (see Discussion for more details). Because both translational energy distributions for C−C fission are peaked away from 0 kcal/mol and have tails which extend to high energy, there must be a barrier to the reverse reaction for both channels. Consideration of the CO_2^+ spectrum alone does not allow us to identify the primary photolytic process(es) which generate the observed signal; it is through analysis of the rest of the data presented herein that we are able to assign all signals in Figure 3 as resulting from

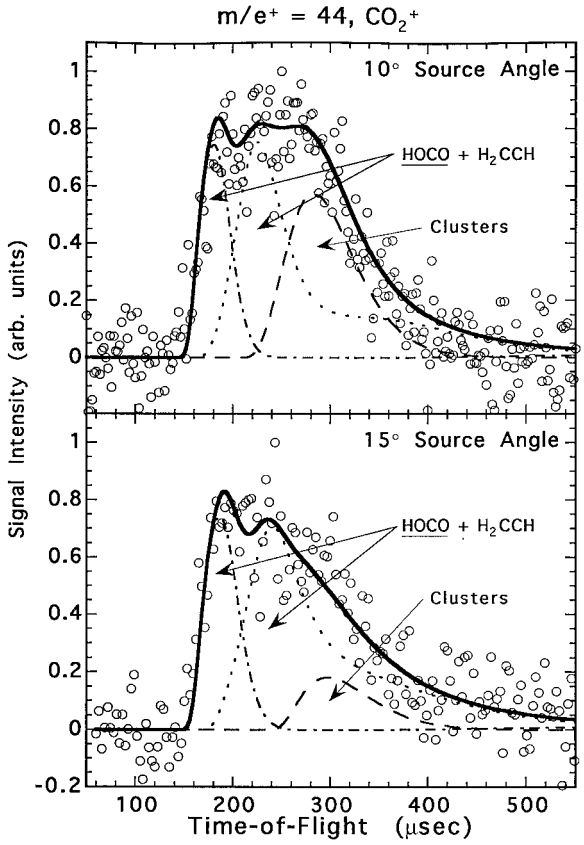

Figure 5. Laboratory time-of-flight spectra of the photofragments detected at CO_2^+ with a nozzle heated to 375 °C at source angles of 10° (top) and 15° (bottom). All early signal results from primary C−C bond fission and is fit with the $P(E_T)$'s shown in Figure 4. Signal at late flight times is due to residual cluster contamination in the molecular beam. The c.m. recoil velocity distribution used to fit the signal from cluster dissociation, as determined from the low nozzle temperature data, is shown in Figure 2.

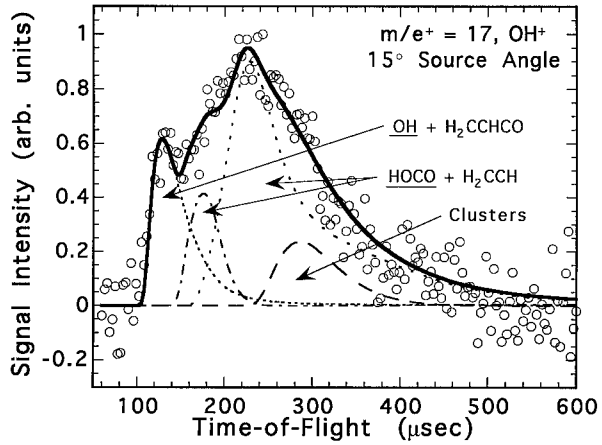

Figure 6. Laboratory time-of-flight spectrum of the photofragments detected at $m/e^+ = 17$, OH^+, with a nozzle heated to 375 °C. The source angle was 15°. The main part of the spectrum results from the OH^+ daughter ion of the HOCO radical produced by primary C−C bond fission and is fit with the $P(E_T)$'s in Figure 4 with a high:low translational energy distribution ratio of 0.86:1.0. A small amount of cluster contamination is also evident at this smaller angle. The fast peak at about 105 μs results from primary C−O bond fission and is fit with the $P(E_T)$ in Figure 7.

primary C−C bond fission (see section D). Figure 5 shows the CO_2^+ signal collected at other source angles: 10° (top) and 15° (bottom). In these spectra the third component to the fits which is needed at late arrival times is due to clusters.

Figure 6 shows the photofragment TOF spectrum taken at $m/e^+ = 17$, OH^+, with a source angle of 15° after 1 000 000 laser shots. The broad peak in the spectrum has the same flight time as the $m/e^+ = 44$, CO_2^+, data in the bottom frame of Figure 5 and is fit with the same C−C fission $P(E_T)$'s (Figure 4). Therefore, this signal must be the OH^+ daughter ion of the HOCO radical. The early part of the spectrum results from a different process and, due to its fast arrival time, must result from a light fragment recoiling from a more massive one. We assign this early signal to primary C−O fission (eq 2), and forward convolution fitting of the fast part of the OH^+ spectrum gives a translational energy distribution (Figure 7) with E_{mean} = 15.6 kcal/mol. Since the $P(E_T)$ is peaked well away from 0 kcal/mol, there must be substantial slope to the electronic surface along the C−O bond fission channel (i.e. a large barrier to the reverse reaction). Figure 8 shows the OH^+ signal collected at different source angles: 10° (top) and 25° (bottom).

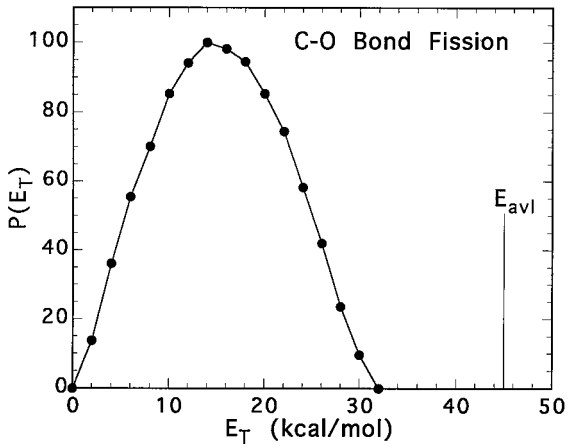

Figure 7. Center-of-mass product translational energy distribution, $P(E_T)$, for the C−O bond fission channel in acrylic acid. The $P(E_T)$ is derived from forward convolution fitting the early portion of the OH^+ signal in Figure 6. The line at 42 kcal/mol represents the energy available after photodissociation based on a C−O bond strength of 106 kcal/mol calculated from heats of formation.[14]

The signal collected at $m/e^+ = 26$, $C_2H_2^+$ (Figure 9) with a 20° source angle after 250 000 laser shots exhibits contributions from both C−C fission channels and the C−O fission channel. The fast shoulder of this signal is due to the $C_2H_2^+$ daughter ion of the C_2H_3 radical which is momentum-matched to the HOCO radical observed in the OH^+ and CO_2^+ spectra and therefore fit with the high-energy $P(E_T)$ in Figure 4. The other C−C fission channel appears as the fast part of the main peak. The slow portion of the main peak is due to the $C_2H_2^+$ daughter ion of the $H_2C{=}CHCO$ fragment which is momentum-matched to the OH radical in Figures 6 and 8. The signal collected at other angles for $m/e^+ = 26$ (Figure 10) and at a 10° source angle for $m/e^+ = 27$, $C_2H_3^+$ (Figure 11), have similar contributions as well as some late signal due to clusters.

Even at high nozzle temperatures, all the ion signal at $m/e^+ = 45$, $HOCO^+$, and $m/e^+ = 55$, $H_2C{=}CHCO^+$, which correspond to parent ions for C−C and C−O fission, respectively, appears to be due to clusters. This is a result of fragmentation in the ionizer and is not entirely surprising considering that many of the photodissociation products have large amounts of internal excitation and we use 200 eV electrons to accomplish ionization. There is also the problem that slow moving $H_2C{=}CHCO$ radicals arrive at times similar to fragments resulting from cluster photodissociation; thus, any signal in the $m/e^+ = 55$ spectra resulting from C−O bond fission may be obscured by the presence of clusters. While the inability to detect the monomer photodissociation signal at $m/e^+ = 45$ or $m/e^+ = 55$ complicates the assignment of dissociation channels, it does not affect the conclusions herein because of the wealth of information gained from other spectra.

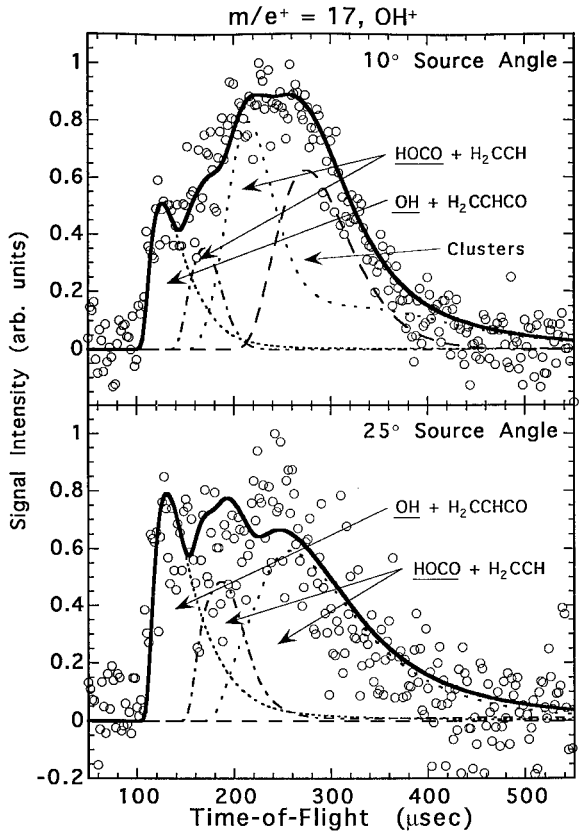

Figure 8. Laboratory time-of-flight spectra of the photofragments detected at OH^+ with a nozzle heated to 375 °C at source angles of 10° (top) and 25° (bottom). All the signal is fit with the same components used in Figure 6. Due to their small recoil angle from the interaction region, photofragments from cluster dissociation are not observed in the bottom frame but are present in the data collected at 10° (top).

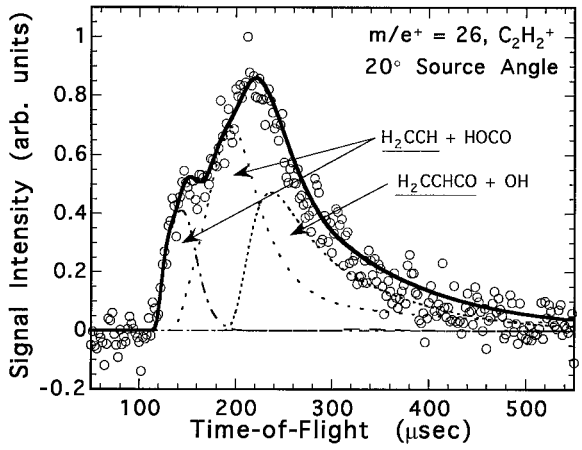

Figure 9. Laboratory time-of-flight spectrum of the photofragments detected at $m/e^+ = 26$, $C_2H_2^+$, with a nozzle heated to 375 °C. The source angle was 20°. The fast part of the spectrum results from the C_2H_3 radical produced by primary C−C bond fission and is fit with the $P(E_T)$'s in Figure 4 with a high:low translational energy distribution ratio of 1.0:1.0. The slow edge results from daughter ions of $H_2C{=}CHCO$ radicals produced by primary C−O bond fission and is fit with the $P(E_T)$ in Figure 7.

C. Uncovering Small Amount of Signal from Monomers. *Dissociation in Low-Temperature Nozzle Data.* Now that we have identified C−C and C−O fission as primary photodissociation channels in acrylic acid and know the translational energy distributions associated with each process, we can fit the small monomer signal observed using a low-temperature nozzle to check for consistency. Figure 12 shows photofragment TOF spectra taken at $m/e^+ = 44$, CO_2^+ (top) and $m/e^+ = 17$, OH^+ (bottom) with a source angle of 10°. The large, broad peaks are entirely due to clusters. In the CO_2^+ spectrum, the signal at 200 μs results from monomer C−C bond fission as in Figures 3 and 5. Although the signal resulting from monomer dissociation is comparable to that from clusters in this spectrum, this is the only mass/charge ratio where this is true; the OH^+ signal in the lower frame is more typical of the data collected with a 120 °C nozzle temperature. In the bottom frame of Figure 12, the small amount of signal at early flight times is fit with C−O and C−C fission $P(E_T)$'s just as the $m/e^+ = 17$ signal in Figures

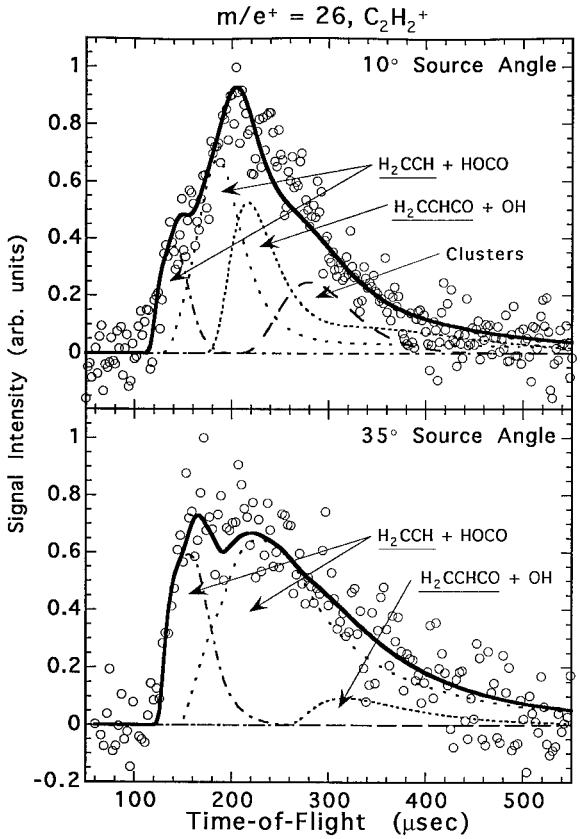

Figure 10. Laboratory time-of-flight spectra of the photofragments detected at $C_2H_2^+$ with a nozzle heated to 375 °C at source angles of 10° (top) and 35° (bottom). All signal is fit by primary C−C and C−O bond fission channels, with cluster contamination evident at the smaller source angle in the top frame.

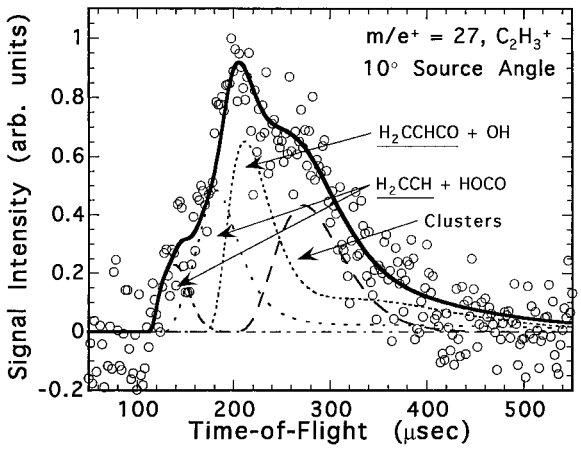

Figure 11. Laboratory time-of-flight spectrum of the photofragments detected at $m/e^+ = 27$, $C_2H_3^+$, with a nozzle heated to 375 °C. The source angle was 10°. The fast edge of the spectrum results from the C_2H_3 radical produced by primary C−C bond fission and is fit with the $P(E_T)$'s in Figure 4 with a high:low translational energy distribution ratio of 1.0:1.0. The large peak at 180 μs results from $H_2C{=}CHCO$ radicals produced by primary C−O bond fission and is fit with the $P(E_T)$ in Figure 7. Again, the late signal is due to cluster contamination.

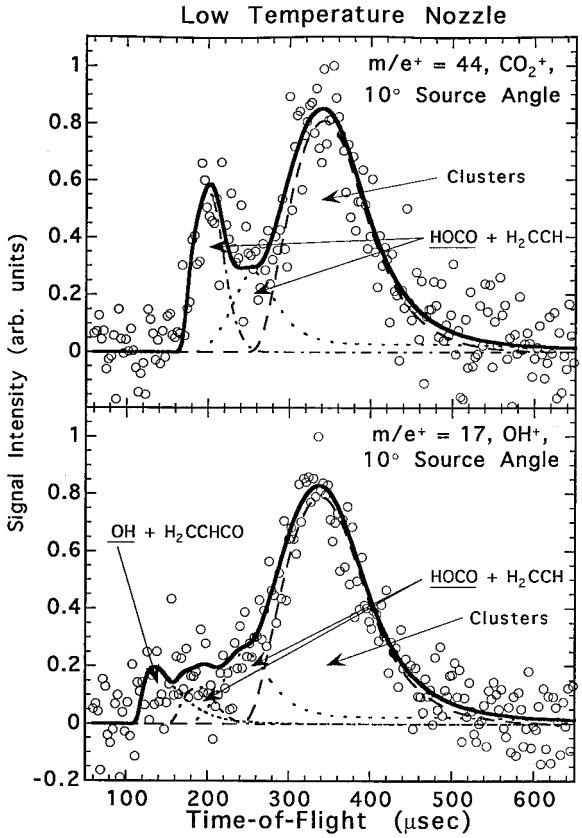

Figure 12. Laboratory time-of-flight spectrum of the photofragments detected at CO_2^+ (top) and OH^+ (bottom) with a nozzle heated to 120 °C. The source angle was 10°. The large peak at 330 μs in both spectra is due entirely to clusters. In the top frame, the smaller, faster peak results from primary C−C bond fission in the monomer and is fit with the $P(E_T)$'s in Figure 4. In the bottom frame, the large peak is again due to the signal from cluster dissociation. The small amount of early signal is quite noisy but is simulated relatively well by inclusion of the C−C and C−O bond fission channels used to fit the OH^+ spectra in Figures 6 and 8. In order to fit both spectra in this figure, we had to slightly modify the relative weightings of the channels from those used to fit the corresponding 375 °C nozzle temperature data. This could be due to either different daughter ion production probabilities or subtle differences in $P(E_T)$'s caused by using two extremely different temperatures.

6 and 8. Here we have used approximately the same relative weightings between dissociation channels as in the data collected with a 375 °C nozzle temperature (the ratios of high:low energy C−C fission distributions are 2.5:1.0 for the CO_2^+ data and 0.94:1.0 for the OH^+ data), with the ratio of cluster to monomer contributions increased by a factor of about 3, the increase in cluster contribution we observe from parent beam TOF measurements. The $m/e^+ = 17$ data represents the signal collected after 2 000 000 laser shots, and the primary dissociation channels are barely visible above the background. It would have been impossible to fit this data in a reliable manner if we did not already know the translational energy distributions for the various processes. Using the results obtained at 375 °C, however, we obtain a good fit to this data, illustrating that the same photodissociation dynamics are occurring at lower temperatures.

D. Assignment of Dissociation Channels. Due to the large amount of ionizer-induced fragmentation and the multiple channels involved in the photodissociation of acrylic acid, clear assignments of the dissociation pathways cannot be made unless all the data is considered as a whole. For example, the $m/e^+ = 44$ signal could, theoretically, be attributed to three different ions: the CO_2^+ daughter ion of HOCO radicals produced from C−C fission, CO_2^+ parent ion resulting from decarboxylation (eq 3), or $H_2C{=}CHOH^+$ parent ion resulting from decarbonylation (eq 4). Since both translational energy distributions that comprise the $m/e^+ = 44$ signal appear with the same flight times in the $m/e^+ = 17$ spectra, however, the decarboxylation reaction can be eliminated from consideration as a component of the $m/e^+ = 44$ spectra (neither CO_2 nor $H_2C{=}CH_2$ radicals can give ion signal at $m/e^+ = 17$). We eliminate vinyl alcohol, $H_2C{=}CHOH^+$, as a possibility, because even though this species could give a signal at $m/e^+ = 44$ and $m/e^+ = 17$ (the OH^+ daughter), it would not give a momentum-matched signal at $m/e^+ = 27$ or $m/e^+ = 26$ since the recoil partner in the dissociation process is CO. To the contrary, if the signal we attribute to C−C bond fission was actually from $H_2C{=}CHOH$, the signal at $m/e^+ = 27$ and $m/e^+ = 26$ would have the same flight times as the signal seen at $m/e^+ = 17$ and $m/e^+ = 44$ since $H_2C{=}CHOH$ can yield a signal at all four mass/charge ratios. For these reasons we can firmly say that both energy distributions in Figure 4 are due to primary C−C bond fission despite the fact that the HOCO product does not give a significant signal at the $HOCO^+$ parent ion upon 200 eV electron bombardment ionization.

We identify the fast component of the $m/e^+ = 17$, OH^+, spectrum in a similar manner. This assignment is made easier by the fact that only OH^+ has a mass/charge ratio of 17 in this experiment. Since the fast translational energy distribution which fits this portion of the signal does not appear in the $m/e^+ = 44$ spectra, it is not from a HOCO radical daughter ion. Also, since its momentum-matched partner appears at $m/e^+ = 27$ and $m/e^+ = 26$, the OH^+ signal cannot be due to vinyl alcohol for reasons the same as those discussed above for the C−C fission channel. This means the only reasonable source for the fast signal in the OH^+ spectra is from primary C−O bond fission.

Since all the ion signal can be fit by a combination of the three primary photodissociation channels discussed above and the signal due to residual clusters in the beam, molecular CO_2 (decarboxylation) and CO elimination (decarbonylation) are not significant primary dissociation pathways.

E. Why We Must Use Two C−C Fission $P(E_T)$'s. We use two translational energy distributions to describe primary C−C fission because it is not possible to fit the various spectra with one consistent energy distribution. In the CO_2^+ data the relative weighting of the high:low energy C−C fission $P(E_T)$'s is approximately 2.0:1.0. When this ratio is used to fit the OH^+ spectrum, there is too much contribution from the high-energy distribution. It is necessary to use a ratio of 0.86:1.0 in order to obtain a good fit to this data. Likewise, the 2.0:1.0 high:low translational energy distribution ratio is too large for $C_2H_3^+$ and $C_2H_2^+$ data which require ratios of 1.0:1.0. This variation in the ratio of the high:low translational energy distributions for C−C fission is an indication that the daughter ion fragmentation patterns for ground state and electronically excited HOCO radicals are different. It is well documented that internal excitation of radicals can greatly effect the ionization-induced fragmentation pattern, even when very high ionization energies are used,[15] so it is not surprising that electronically excited HOCO radicals have a different daughter ion fragmentation pattern than ground electronic state HOCO radicals. Because we do not know what the daughter ion fragmentation patterns are for the various radicals produced in the photodissociation of acrylic acid, we can neither determine an absolute C−C:C−O fission branching ratio nor even give a qualitative measure of which channel is dominant. We also must note that since the two C−C fission energy distributions overlap, there is some uncertainty regarding the overlapping regions. That is, part of the high-energy tail of the low-energy distribution may actually be associated with the high-energy distribution. This is a subtle

matter, however, and does not effect the general conclusions of this paper.

Discussion

Upon 193 nm irradiation of acrylic acid monomers we only observe products which result from primary C−O and C−C bond fission. Although there are no prior comprehensive studies of the photodissociation dynamics of acrylic acid at this wavelength, other researchers have indicated that decarboxylation and decarbonylation reactions are significant primary processes. This is contrary to our findings. In one such study, Miyoshi and co-workers[3] observed a signal at $m/e^+ = 44$ after 193 nm photolysis of acrylic acid. Their assignment of this signal to vinyl alcohol (the momentum-matched partner to CO elimination) appears to be in error, and the signal is actually from the CO_2^+ daughter ion of the HOCO radical.

The most compelling evidence for CO and CO_2 elimination processes comes from spectroscopic studies. After 193 and 248 nm irradiation of low-pressure gas-phase acrylic,[9] methacrylic,[9] and pruvic[16] acids, Rosenfeld and Weiner reported intense infrared fluorescence at 4.3 μm (2319 cm^{-1}) corresponding to $\Delta v = -1$ transitions in the asymmetric stretch mode of CO_2. They attributed this observation to photodecarboxylation reactions in all three molecules. More recent studies by Lessard and Rosenfeld[17] measure the high-resolution infrared spectra of CO and CO_2 from acrylic acid dissociated at 193 and 248 nm. Since their detection method is very sensitive to any CO or CO_2 produced, they would observe even the smallest amounts of these products. Since we do not observe either of these species as direct photolysis products, our data show the overall yield of CO and CO_2 as primary photofragments must be minimal compared to C−O and C−C bond fission products. Another possible explanation is that the CO and CO_2 products observed by Lessard and Rosenfeld resulted from cluster dissociation because they used a total acrylic acid pressure of 100 to 200 mTorr; this pressure can result in significant amounts of cluster contamination.

Although we do not have enough experimental evidence to precisely describe the mechanisms involved in C−C and C−O primary bond fission in acrylic acid, we can make some preliminary conclusions based on the work herein and experiments performed on similar systems by others. The presence of two distinct translation energy distributions for C−C fission indicates there are two different pathways to C−C fission. One imparts only small amounts of translational energy, and the other yields fragments with a large portion of the available energy in translation. Two distinct A-B bond fission energy distributions usually result because one of the photofragments, in this case either the HOCO or C_2H_3 radical, is produced in both the ground and an electronically excited state. We must assign the low kinetic energy distribution channel to the formation of electronically excited HOCO because the first excited state the vinyl radical, $C_2H_3(\tilde{A})$, is approximately 46 kcal/mol higher in energy than the ground state of the C_2H_3 radical.[18] This would only leave 8 kcal/mol of energy to be distributed among internal and translational degrees of freedom. Even the low-energy C−C fission translational energy distribution in Figure 4 requires more energy than is available if $C_2H_3(\tilde{A})$ is produced.

The energy of the first excited state of the HOCO radical is not well-known. One estimate of the excited state energy is about 36 kcal/mol.[19] Although this energy is only a rough estimate and may be in error by 5 kcal/mol or more, it is lower than the energy for the $\tilde{A}$ state of the C_2H_3 radical thus allowing more energy (18 kcal/mol) for translation of the photofragments. Figure 4 shows that the low translational energy distribution has a tail that extends to beyond 18 kcal/mol, but, as noted in section III.E, there is uncertainty associated with the overlapping portions of these distributions. It is very possible that there is a sharp truncation of the lower energy distribution near 18 kcal/mol and the high-energy portion of the distribution is actually part of the high-energy distribution. Since the C−C bond energy, energy of the first excited state of the HOCO radical, and overlapping portions of the C−C translational energy distributions are all approximate within a few kcal/mol, it appears that the slower moving fragments result from a pathway which produces ground state C_2H_3 and electronically excited HOCO radicals.

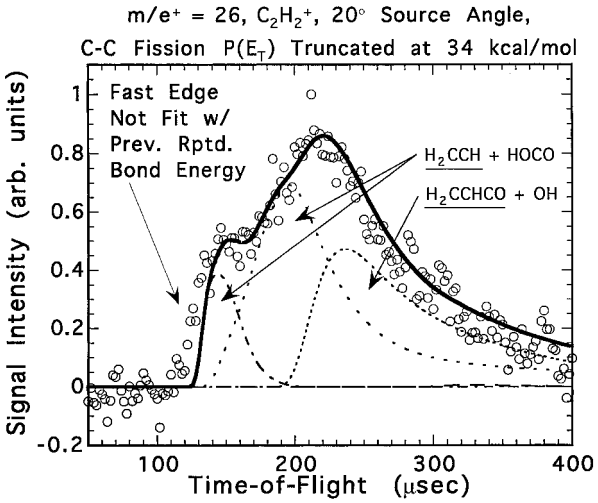

Figure 13. Laboratory time-of-flight spectrum of the photofragments detected at $C_2H_2^+$ with a nozzle heated to 375 °C. The source angle was 20°. This is the same data presented in Figure 9, but in fitting this spectrum, we have truncated the high-energy C−C bond fission channel from Figure 4 at 34 kcal/mol as suggested by the C−C bond dissociation energy of 114 kcal/mol reported by Petty and co-workers.[2] Clearly, data with early flight times is not fit unless the $P(E_T)$ extends to higher energies; thus D_0(C−C) must be less than approximately 100 kcal/mol.

It is apparent that both the HOCO and the vinyl radical from the photodissociation of acrylic acid are formed with low internal energies which leave them stable to secondary unimolecular dissociation. C_2H_3 can dissociate to C_2H_2 + H with internal energies above 35.7 kcal/mol,[20] but the available energy in the photodissociation to C_2H_3 + ground state HOCO is largely partitioned to kinetic energy of the recoiling fragments, not to internal energy of the C_2H_3 or HOCO fragments. (Fewer than 10% of the C_2H_3 photofragments would, by virtue of their low kinetic energy, have enough internal energy to undergo secondary dissociation.) For the second channel producing electronically excited HOCO, we observe a signal from HOCO at both CO_2^+ and OH^+, so that the kinetic energy distribution must result from electronically excited HOCO that does not dissociate unimolecularly before reaching our ionizer. Since we can fit the HOCO signal and the momentum-matched C_2H_3 signal with the same kinetic energy distribution, no significant part of the slowly recoiling HOCO fragments undergoes secondary dissociation.

The high-energy translational energy distribution also warrants further comment. Previous researchers have suggested that the C−C bond strength in acrylic acid is as high as about 114 kcal/mol.[2] This would leave only about 34 kcal/mol of energy to be distributed between relative product translational energy and internal excitation of the photofragments. Figure 4 clearly shows that we see HOCO and C_2H_3 radicals with relative translational energy which extends to 50 kcal/mol. If we truncate this energy distribution at 34 kcal/mol, we cannot fit the fast edge of the $m/e^+ = 26$, $C_2H_2^+$, spectrum as shown in Figure 13. Apparently, Petty and co-workers[2] assumed too

much resonance stabilization due to the conjugated π electrons. We base the C−C bond energy of 94 kcal/mol on literature heats of formation.[14] While this value may be in error by several kcal/mol, the high-energy tail to the C−C fission translational energy distribution clearly indicates the C−C bond strength is weaker than the previously estimated value of 114 kcal/mol; our data shows it has a maximum value of about 100 kcal/mol.

Although our experimental data does not determine the type of dissociation mechanism, C−C and C−O bond fission do not occur solely along the initially excited $\pi\pi^*$ electronic state (S_2) because the S_2 state does not correlate adiabatically to ground state C−C or C−O fission products. In acrylic acid, $\pi\pi^*$ excitation results in a charge transfer state which has double-bond character along the C−C bond connecting the vinyl and carbonyl groups.[21] Since acrolein ($H_2C{=}CHCOH$) exhibits similar electron transfer characteristics when excited at 193 nm, the two molecules probably have similar photodissociation dynamics. In fact, two studies[5,6] have observed C−C and aldehydic C−H fission in acrolein which are pathways analogous to the C−C and C−O bond fission channels found in acrylic acid (the bonds that break are in α positions to the carbonyl). They also assign a decarbonylation channel which does not occur to a significant extent in acrylic acid photodissociation at 193 nm. Partly on the basis of fragment anisotropy measurements, it is generally accepted that acrolein photodissociation occurs via rapid radiationless transitions to lower-lying electronic states (both excited singlet and triplet states may be involved, as well as the ground electronic state) from the initially prepared S_2 state.[5−7] It is logical that acrylic acid excited at 193 nm dissociates in the same manner. Because there are significant amounts of translational energy imparted to all the photofragments by the dissociation event in acrylic acid, there must be a barrier to the reverse reactions. For this reason, C−C or C−O bond fission after internal conversion to the ground electronic state is not a mechanism consistent with the acrylic acid experimental data. In order to fully elucidate the mechanism(s) involved in acrylic acid photodissociation, however, high-level *ab initio* potential energy surfaces are necessary.

Summary

We observe both primary C−C and C−O bond fission in acrylic acid after excitation to the $\pi\pi^*$ state with 193 nm light. Primary C−C fission producing C_2H_3 and HOCO radicals appears to occur via two different pathways as indicated by the presence of two different relative translational energy distributions for these products. One of the C−C fission channels yields electronically excited HOCO which accounts for the products having a small amount of translational energy. Both C−C and C−O bond fission impart large amounts of energy into relative fragment translation, suggesting these processes occur on electronically excited state potential energy surfaces since simple bond fission in the ground electronic state is generally barrierless. Because we observe some C−C fission products with translational energies as high as 50 kcal/mol, we determine the upper limit of the C−C bond strength to be about 100 kcal/mol, which is in reasonable agreement with bond strength calculations based on heats of formation. Since there are competing dissociation processes when acrylic acid is excited at 193 nm, this is probably not the most favorable means of producing the HOCO radical, especially since many of the HOCO radicals are produced with large amounts of internal energy. Further research, such as product distribution anisotropy measurements and *ab initio* excited state potential energy surface calculations, on acrylic acid and similar compounds are necessary in order to better understand the dissociation dynamics of this molecule.

Acknowledgment. This work was supported by the Division of Chemical Sciences, Office of Basic Energy Sciences, Office of Energy Research, U.S. Department of Energy, under Grant DE-FG02-92ER14305. D.C.K.'s stipend and tuition were supported by a U.S. Department of Education GAANN fellowship during a portion of this work. N.R.F. thanks NSERC for a 1967 Science and Engineering Scholarship. We thank Prof. Peter Kelly for providing us with a copy of the Lessard thesis given in ref 17. L.J.B. expresses her deepest gratitude to Yuan T. Lee, who was the finest colleague and scientific father in his role as Ph.D. advisor to her and so many others.

References and Notes

(1) See, for example: Sears, T. J.; Fawzy, W. M.; Johnson, P. M. *J. Chem. Phys.* **1992**, *97*, 3996.

(2) See, for example: Petty, T. J.; Harrison, Moore, C. B. *J. Phys Chem.* **1993**, *97*, 11194.

(3) Miyoshi, A.; Matsui, H.; Washida, N. *J. Chem. Phys.* **1994**, *100*, 3532.

(4) Forman, R. L.; Mackinnon, H. M.; Ritchie, P. D. *J. Chem. Soc. C* **1968**, 2013.

(5) Hass, B. M.; Minton, T. K.; Felder, P.; Huber, J. R. *J. Phys. Chem.* **1991**, *95*, 5149.

(6) Shinohara, H.; Nishi, N. *J. Chem. Phys.* **1982**, *77*, 234.

(7) Lessard, P. C.; Rosenfeld, R. N. *J. Phys. Chem.* **1992**, *96*, 4615.

(8) Singleton, D. L.; Paraskevopoulos, G.; Irwin, R. S. *J. Phys. Chem.* **1990**, *94*, 695.

(9) Rosenfeld, R. N.; Weiner, B. R. *J. Am. Chem. Soc.* **1983**, *105*, 6233.

(10) Lee, Y. T.; McDonald, J. D.; LeBrenton, P. R.; Herschbach, D. R. *Rev. Sci. Instrum.* **1969**, *40*, 1402. Wodtke, A. M.; Lee, Y. T. *J. Phys. Chem.* **1985**, *89*, 4744. Person, M. D. Ph.D. Thesis, Department of Chemistry, University of Chicago, 1991.

(11) *Encyclopedia of Chemical Technology*, 3rd ed.; Wiley: New York, 1984; p 363.

(12) Feng, W. Y.; Lifshitz, C. *J. Phys. Chem.* **1994**, *98*, 6075.

(13) Chao, J.; Zwolinski, B. J. *J. Phys. Chem. Ref. Data* **1978**, *7*, 363.

(14) The heats of formation used are $\Delta H_f°$(acrylic acid) = −76.6 kcal/mol (Vilcu, R.; Perisanu, S. *Rev. Roum. Chim.* **1980**, *25*, 619), $\Delta H_f°$-($H_2C{=}CH$) = 71 kcal/mol (ref 18), and $\Delta H_f°$(OH) = 9.4 kcal/mol, $\Delta H_f°$(HOCO) = −53.3 kcal/mol, and $\Delta H_f°$($H_2C{=}CHCO$) = 17.3 kcal/mol (McMillen, D. F.; Golden, D. M. *Annu. Rev. Phys. Chem.* **1982**, *33*, 493). All of these values are at 298 K; the correction to 0 K is generally less than a couple of kcal/mol and falls within experimental error of reported values.

(15) See, for example, how the NO_2 fragmentation pattern used (Davis, H. F.; Kim, B.; Johnson, H. S.; Lee, Y. T. *J. Phys Chem.* **1993**, *97*, 2172) to get absolute branching ratios varies when the NO_2 product is produced vibrationally hot in: Butler, L. J.; Krajnovich, D.; Lee, Y. T.; Ondrey, G.; Bersohn, R. *J. Chem. Phys.* **1983**, *79*, 1708.

(16) Rosenfeld, R. N.; Weiner, B. R. *J. Am. Chem. Soc.* **1983**, *105*, 3485.

(17) Lessard, P. C. Ph.D. Thesis, University of California, Davis, 1990.

(18) Wodtke, A. M.; Hintsa, E. J.; Somorjai, J.; Lee, Y. T. *Isr. J. Chem.* **1989**, *29*, 383.

(19) Sears, T. J.; Radford, H. E.; Moore, M. A. *J. Chem. Phys.* **1993**, *98*, 6624.

(20) Ervin, K. M.; Gronert, S.; Barlow, S. E.; Gilles, M. K.; Harrison, A. G.; Bierbaum, V. M.; DePuy, C. H.; Lineberger, W. C.; Ellison, G. B. *J. Am. Chem. Soc.* **1990**, *112*, 5750. Harding, L. B.; Wagner, A. F.; Bowman, J. M.; Schatz, G. C.; Christoffel, K. *J. Phys. Chem.* **1982**, *86*, 4312.

(21) Arendt, M. F.; Browning, P. W.; Butler, L. J. *J. Chem. Phys.* **1995**, *103*, 5877. Nagakura, S. *Mol. Phys.* **1960**, *3*, 105.